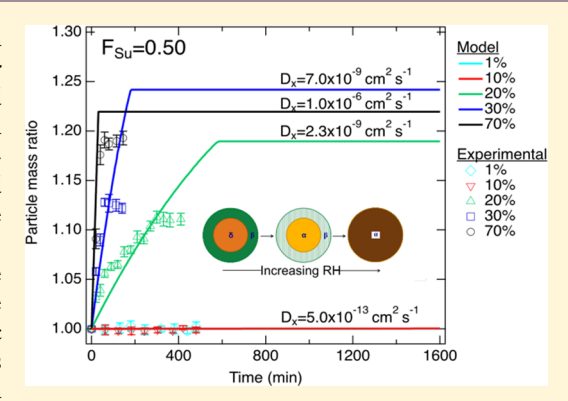


# Effects of Phase State and Phase Separation on Dimethylamine Uptake of Ammonium Sulfate and Ammonium Sulfate—Sucrose Mixed Particles

Wing-Sy Wong DeRieux,<sup>†,⊥</sup> Pascale S. J. Lakey,<sup>†,⊥</sup> Yangxi Chu,<sup>‡</sup> Chak K. Chan,<sup>§</sup> Hayley S. Glicker,<sup>†</sup> James N. Smith,<sup>†</sup> Andreas Zuend, and Manabu Shiraiwa\*,<sup>†</sup>

Supporting Information

ABSTRACT: Unexpectedly high amounts of aminium salts have been detected in ambient aerosol particles, prompting investigations into their role in new particle formation and nanoparticle growth. Amine uptake and particle-phase processes, including the effects of phase state and non-ideal mixing, are poorly understood. In this study, we conducted kinetic multilayer modeling of dimethylamine (DMA) uptake by crystalline and aqueous ammonium sulfate (AS) and mixed ammonium sulfate—sucrose particles based on measurements at different relative humidity (RH) values. The temporal evolution of particle mass increases and the humidity dependence were successfully reproduced by considering the amine/ammonium exchange reaction and formation of hygroscopic dimethylaminium sulfate. Thermodynamic equilibrium predictions suggest that aqueous sucrose and AS mixtures undergo phase separation at RH < 94%. The kinetic model simulations reveal that DMA uptake is



limited by diffusion of DMA and AS through a viscous sucrose-rich shell at lower RH, resulting in strong concentration gradients in the particle bulk. The model predicts that the true uptake coefficients would range from  $2.0 \times 10^{-5}$  to  $2.6 \times 10^{-3}$  for initially solid particles at low RH, while they can be as high as 0.70-0.82 in aqueous particles at high RH. Uptake coefficients increase when RH and associated particle water content increase, while they generally decrease when the molar fraction of sucrose increases at a specific value of RH. Using new measurements of ambient amines from the Holistic Interactions of Shallow Clouds, Aerosols and Land Ecosystems (HI-SCALE) field campaign as a reference, the model is extrapolated to particles with a diameter of 30 nm and amine mixing ratios in the ppt range to emulate atmospheric conditions. At 70% RH or higher with particles in the liquid phase, amine uptake can lead to a mass increase of approximately 20-60%.

KEYWORDS: kinetic modeling, nanoparticle growth, non-ideal thermodynamic mixing, aminium salts, amorphous semi-solid state

# **■** INTRODUCTION

Atmospheric sub-micrometer aerosol particles play an important role in air quality, climate, and public health. <sup>1–3</sup> The role of alkyl amines in atmospheric aerosol chemistry is of interest due to the unexpectedly high amounts of aminium salts detected in ambient aerosol particles. <sup>4–11</sup> These amounts are out of proportion to the relative amounts of amine and ammonia detected in the atmosphere, since small-chain alkyl amines are typically present at concentrations several orders of magnitude lower than that of ammonia in the gas phase. <sup>12</sup> Ammonia is known to form or contribute substantially to inorganic aerosols by neutralizing atmospheric acids, while amines are receiving growing attention for their potential role in new particle formation.

One pathway through which amines partition from the gas phase into particles is reactive uptake by ammonium sulfate (AS) aerosols. Various studies have reported the displacement of ammonium by an alkylaminium ion. Earlier reports investigated the reaction at low pressure under conditions with limited water. Qiu et al. (2011) studied the heterogeneous uptake of methylamine, dimethylamine (DMA), and trimethylamine vapor by AS and ammonium bisulfate coatings on glass tubes at low pressure and low RH,

Special Issue: New Advances in Organic Aerosol Chemistry

Received: May 16, 2019 Revised: June 11, 2019 Accepted: June 17, 2019 Published: June 17, 2019



<sup>&</sup>lt;sup>†</sup>Department of Chemistry, University of California, Irvine, California 92697-2025, United States

<sup>&</sup>lt;sup>‡</sup>Chinese Research Academy of Environmental Sciences, Beijing 100012, China

<sup>§</sup>School of Energy and Environment, City University of Hong Kong, Hong Kong, China

Department of Atmospheric and Oceanic Sciences, McGill University, Montreal, QC H3A 0B9, Canada

reporting initial uptake coefficients of  $(2.6-3.4) \times 10^{-2}$  and steady-state uptake coefficients of  $(2.3-60) \times 10^{-4}$ . Liu et al.  $(2012)^{14}$  studied the displacement of ammonium from various powdered ammonium salts by aqueous methylamine vapor at very low pressure to report uptake coefficients ranging from 2.3  $\times 10^{-3}$  to  $1.8 \times 10^{-2}$ .

Several studies have reported investigations of amine uptake reactions by AS and other particles. Chu and Chan (2017)<sup>18</sup> reported measurements of the reactive uptake of DMA by crystalline or aqueous AS and AS-sucrose mixed particles. The net reaction is

$$(CH_3)_2NH(g) + NH_4^+(aq) \rightarrow$$
  
 $(CH_3)_2NH_2^+(aq) + NH_3(g)$  (1)

They performed their experiments under conditions of controlled relative humidity (RH) and observed that the amine/ammonium exchange reaction appeared to be water and bulk diffusion limited. Chu and Chan<sup>18</sup> also reported visual observations and Raman spectroscopic data consistent with the presence of liquid—liquid phase separation in their mixed ammonium sulfate—sucrose micrometer-sized particles. Sucrose is a widely used surrogate for the hydrophilic organic component of secondary organic aerosol (SOA) particles.

SOA can adopt liquid, semi-solid, or glassy phase states depending on chemical composition, temperature, and RH. 19-23 Phase state and associated particle viscosity may affect crucial atmospheric aerosol processes such as ice nucleation,<sup>24</sup> gas uptake, and particle growth in terms of both magnitude and characteristic time scales. 25 The presence of a viscous semi-solid or glassy phase state can limit reactive uptake by reducing mass transfer and bulk diffusion in aerosol particles. 26-32 Particle morphology is another important factor affecting uptake processes. It has traditionally been assumed that aerosol particles are homogeneously well-mixed. However, phase separation into two or more liquid or viscous amorphous phases has been observed both in aerosol particles containing organic and inorganic components mixed with water, as well as in electrolyte-free aqueous organic particles.33-38 Phaseseparated particles can adopt either a core-shell morphology, in which one phase completely engulfs a second phase, or a partial-engulfing structure, in which both phases maintain direct contact with the gas phase over some surface area.3 Several studies have demonstrated that the presence of an SOA coating on particles in a core-shell morphology will lead to a substantial decrease in the uptake of gaseous species. 40-42

In this study we investigate the amine/ammonium displacement reaction in particles containing different morphologies and phases using kinetic and thermodynamic modeling to further constrain the reaction mechanism and develop an understanding of limiting processes. A kinetic multi-layer model facilitates the systematic investigation of the reaction over a range of particle sizes, compositions, and environmental conditions. Such information can be useful in setting up future experiments and helps in determining priorities for field measurements.

# ■ METHODS

**Summary of Previous Experimental Work.** Our model was applied to previously reported experimental data from Chu and Chan (2017),<sup>18</sup> briefly described in the following. A single particle was generated from aqueous solutions of AS and sucrose before each individual experiment with the following

sucrose molar fractions on a dry basis:  $F_{\rm Su}=0.00$ , 0.15, 0.28, and 0.50. Particles were levitated in an electrodynamic balance (EDB), and their dry diameters were recorded after drying at low RH (<5%). Each particle was then equilibrated at a specified RH value (RH < 5% and RH = 10, 20, 30, and 70%) in the EDB at a temperature of 297  $\pm$  1 K. Initial particle diameters were in the range of 37–71 mm. Output from the EDB was recorded during exposure to a constant flow of DMA (1 ppm) gas to determine changes in particle mass, size, phase state, and chemical composition due to DMA uptake. Particles were characterized with a Raman spectroscopic system coupled to the EDB. After each experimental run, particles were dried and visually inspected under a microscope.

**Model Description.** Kinetic modeling was utilized to investigate the reactive uptake of DMA by AS and mixed AS-sucrose particles. The change in mass of each particle, expressed as the ratio of the particle mass at each time point relative to its initial mass, was simulated using the kinetic multi-layer model of gas—particle interactions in aerosols and clouds (KM-GAP).<sup>43</sup> Schematics of the kinetic model are provided in Figure 1. For the simulation of single-particle

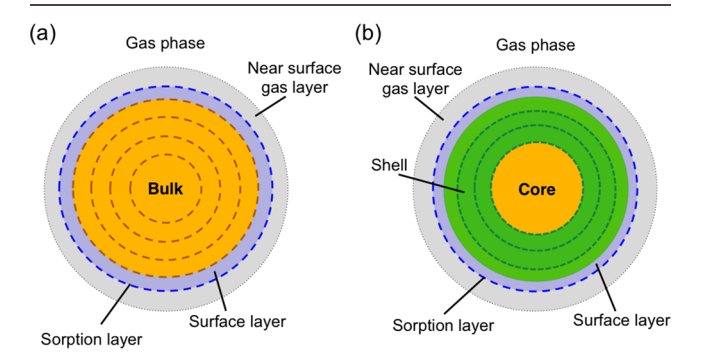


Figure 1. Schematics of the kinetic multi-layer model of gas—particle interactions (KM-GAP) for (a) ammonium sulfate (AS) particles and (b) mixed AS-sucrose particles. The sorption layer is represented by the blue dashed line. In the mixed particles, the core is treated with an AS-rich phase that is either crystalline or aqueous depending on RH, and the shell is initialized as a sucrose-rich phase based on phases and composition data from experiments as well as predictions from AIOMFAC-based equilibrium thermodynamics.

experiments from Chu and Chan (2017), <sup>18</sup> a spherical geometry was applied. The model treats the gas phase with two layers: a quasi-continuous gas-phase layer and a near-surface gas-phase layer. Multiple layers represent the condensed phase: sorption layer, surface layer, and a variable number of bulk layers. KM-GAP treats the following mass transport processes explicitly: gas-phase diffusion, adsorption and desorption, surface—bulk exchange, and bulk diffusion. The chemical reaction (1) was treated in the surface and bulk layers. The model layer thicknesses changed as the simulation experiment proceeded due to solvation of DMA, mass transport between layers, and the conversion of reactants into products, leading to particle growth.

Model Components and Treatment of Particulate Water. For the pure AS particles (Figure 1a), the model treats the reactants and products (ammonia and dimethylaminium sulfate (DMAS)) of the DMA/AS exchange reaction. For the mixed particles, sucrose is also included. AS, DMAS, and sucrose are hygroscopic.<sup>44</sup> The number of associated water molecules is related to the amount of each component present

and remains constant at each RH. Since water molecules are expected to remain closely associated with specific components in the model, we chose to associate the mass and volume of water in non-crystalline layers with these components for simplicity rather than treating water explicitly. The amounts of associated water for AS, DMAS, and sucrose are summarized in Table 1. AS and DMAS associated water values were optimized

Table 1. Associated Water Expressed as the Ratio of Water Molecules to Each Molecule of Indicated Component Used in KM-GAP Modeling for Species in Non-crystalline Layers<sup>a</sup>

	relative humidity						
	1%	10%	20%	30%	70%		
AS	$1.0 \times 10^{-2}$	0.1	0.2	0.8	6.4		
DMAS	0.1	1.0	2.1	3.7	11.8		
sucrose	$5.5 \times 10^{-2}$	0.6	1.1	1.8	6.1		

<sup>a</sup>The same AS and DMAS associated water values were used for both AS-only and AS-sucrose mixed particles. For the AS-sucrose mixed particles, water associated with sucrose was calculated to be consistent with mole fractions predicted by AIOMFAC. <sup>45</sup>

for the pure AS particles using the approach from Chu and Chan  $(2017)^{18}$  as a starting point. The same values were also used for the mixed particles. For the mixed AS-sucrose particles, water associated with sucrose was constrained to be consistent with mole fractions determined by the Aerosol Inorganic-Organic Mixtures Functional groups Activity Coefficients (AIOMFAC)-based equilibrium model.<sup>45</sup> We assumed that the associated water on a per-species basis remains approximately unchanged as the reaction proceeds. However, it should be noted that, in principle, the change in molecular compositions of phases and the interactions among all species would affect the equilibrium water content as the reaction proceeds. To treat this, we would require direct coupling of thermodynamic and kinetic models and the inclusion of detailed interactions of all reaction educts and products of amines and other particle constituents, which is beyond the scope of this study and will be the subject of future

Ammonium Sulfate-Only Particles. At RH < 70%, the initial AS particles were observed to exist in crystalline form. <sup>18</sup> Previous studies have shown that there are surface-adsorbed water molecules on AS particles below the deliquescence RH. <sup>44,46,47</sup> The initial thickness of this layer can range from less than one monolayer (on average) to multiple monolayers depending on RH, as summarized in Table 2 and implemented in KM-GAP.

After particle equilibration, the adsorbed water layer would be saturated with AS. Using the associated water ratios in Table 1 with the volume of the surface layer, the initial amount of dissolved AS was calculated. For simplicity, mass transport to and from the bulk was allowed only for AS, so the particle bulk decreased in size as AS reacted and DMAS formed in the

Table 2. Monolayers of Water Present on Ammonium Sulfate at Different RH Values<sup>44</sup>

	RH (%)				
	1	10	20	30	70
monolayers of H <sub>2</sub> O	0.010	0.646	2.575	4.549	3.379

surface layer. At 70% RH the initial phase of the particle was observed to be liquid in experiments. The volumes of the associated water and the measured dry particle radius were combined to determine the initial aqueous particle volume and diameter.

Kinetic parameters are summarized in Tables S1-S3 that include the gas-phase diffusion coefficient  $(D_{\sigma})$ , surface accommodation coefficient on a free substrate  $(a_0)$ , desorption lifetime  $(\tau_d)$ , second-order surface  $(k_{sslr})$ , and bulk reaction rate coefficient  $(k_{br})$  for reaction (1), Henry's law coefficient of DMA in water  $(5.0 \times 10^{-2} \text{ mol cm}^3 \text{ atm}^{-1})$ , <sup>48</sup> and bulk diffusion coefficients (D<sub>b</sub>) for DMA, AS, NH<sub>3</sub>, and DMAS. We assumed  $a_0$  of unity and  $\tau_d$  of nanoseconds for DMA. A firstorder approximation of Fick's diffusion equation using bulk diffusion coefficients was utilized to describe mass transport fluxes between the layers. D<sub>b</sub> values were varied to optimize the model predictions in comparison to the experimental data. For an initially aqueous particle at 70% RH, the chemical reaction would take place in both surface and bulk layers. A secondorder reaction rate coefficient between DMA and NH<sub>4</sub><sup>+</sup> of 1.0  $\times\ 10^{-15}\ cm^{3}\ s^{-1}$  was used, but predicted mass ratios were found to be insensitive in the range from 1.0  $\times$   $10^{-10}$  to 9.0  $\times$  $10^{-17} \ \text{cm}^3 \ \text{s}^{-1}$ . A single bulk layer was sufficient to describe the solid AS particles (RH < 70%), while multiple layers were used for the aqueous bulk at 70% RH. The number of layers was increased until model predictions converged. At 70% RH, experimental data were fitted with a bulk diffusion coefficient of  $5.0 \times 10^{-6} \text{ cm}^2 \text{ s}^{-1}$  for DMA and AS. For RH < 70%, experimental data were fitted with DMA and AS bulk diffusion coefficients ranging from  $1.5 \times 10^{-10}$  to  $1.25 \times 10^{-11}$  cm<sup>2</sup> s<sup>-1</sup>.

Ammonium Sulfate-Sucrose Mixed Particles. Figure 1b shows a schematic of the modeling approach used for the mixed AS-sucrose particles. The modeling approach is consistent with visual observations and Raman spectroscopic data reported by Chu and Chan (2017).<sup>18</sup> They reported stronger C-H stretching signals near the top and bottom of a particle for  $F_{Su}$  = 0.50, RH < 5%, which indicate higher organic content on the outside of the particle, supporting the presence of a sucrose coating. Additionally, they reported microscopic observations of a shiny white layer on the outside of the dried AS-sucrose particles that was not visible on dried AS only particles. Thermodynamic model predictions also suggest that AS-sucrose particles would be phase-separated (see Results section), as also discussed in a previous study. 49 Thus, ASsucrose particles were modeled assuming a viscous, multilayered, sucrose-rich, outer shell and a monolayered AS core at RH < 70% (Figure 1b). Activity coefficients from a thermodynamic model prediction of particle hydration were used to set initial conditions for a solid AS core and semi-solid sucrose shell containing a small amount of dissolved AS. At 70% RH, activity coefficients from the dehydration case (AIOMFAC-based prediction) were used to set initial conditions for a homogeneously mixed aqueous AS core and the viscous, aqueous sucrose shell in KM-GAP. At all RH values below 70%, the DMA/ammonium exchange reaction (1) was considered in the sucrose-rich shell phase and mass transport from/to the core was only considered for AS. For 70% RH, the chemical reaction and diffusion of all components were considered throughout the particle.

Kinetic parameters are listed in Tables S1—S3. The number of layers in the shell was increased until model predictions converged (number of layers >90). For the mixed AS-sucrose particles, initial particle diameters ranged from 37 to 71 mm.

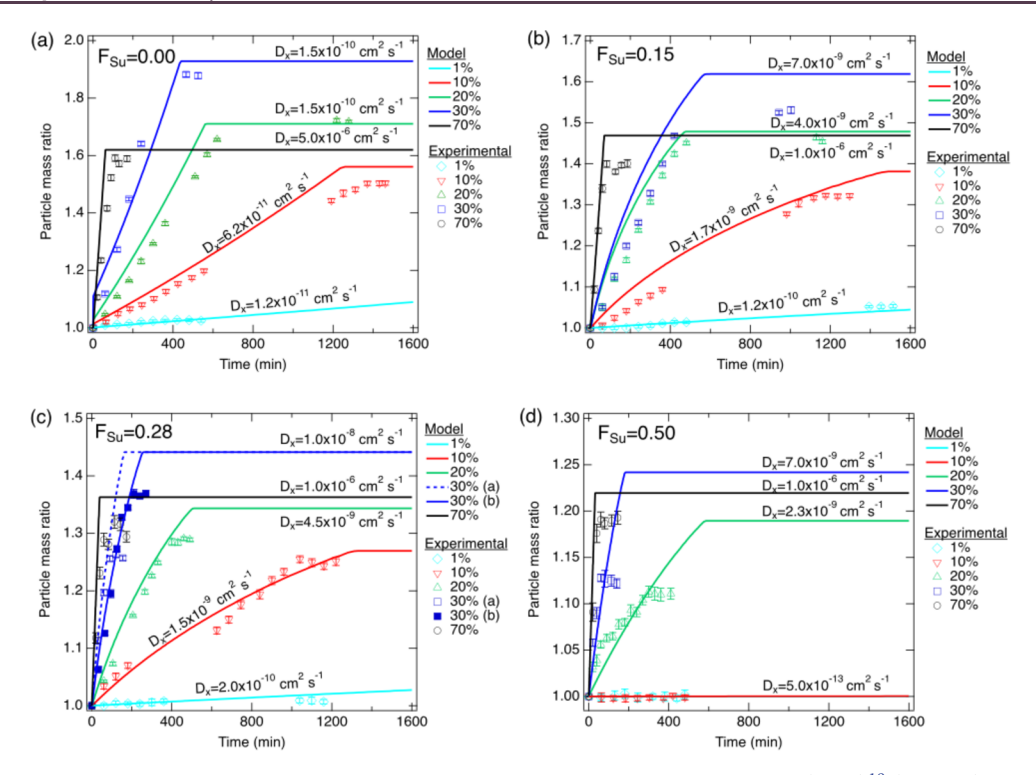


**Figure 2.** Temporal evolution of particle mass ratio upon DMA exposure as measured by Chu and Chan  $(2017)^{18}$  (markers) and simulated by KM-GAP (lines). The sucrose fraction in an AS-sucrose particle is (a)  $F_{Su} = 0.00$  (AS only), (b)  $F_{Su} = 0.15$ , (c)  $F_{Su} = 0.28$ , and (d)  $F_{Su} = 0.50$  at different RH levels of 1% (cyan), 10% (red), 20% (green), 30% (blue), and 70% (black) and a temperature of 297.15 K.

The bulk diffusion coefficients at 70% RH for  $F_{\rm Su} = 0.15$ , 0.28, and 0.50 were set to  $1.0 \times 10^{-6}~{\rm cm}^2~{\rm s}^{-1}$ , consistent with an aqueous particle. For RH < 70%, experimental data were fit well with bulk diffusion coefficients ranging from  $2.0 \times 10^{-10}$  to  $1.0 \times 10^{-8}~{\rm cm}^2~{\rm s}^{-1}$ .

Thermodynamic Modeling. The AIOMFAC thermodynamic group-contribution model, described elsewhere in detail, 45,50 was used to estimate the degree of non-ideal mixing among condensed-phase species in liquid/amorphous phases and to consider the potential for liquid-liquid phase separation within the AS-sucrose system as a function of equilibrium RH. The AIOMFAC-based model employed in this study included a version of the liquid-liquid equilibrium (LLE) algorithm by Zuend and Seinfeld (2013),<sup>51</sup> which predicts the phase compositions of up to two liquid phases for a given overall composition of a mixture based on the activity coefficients computed by AIOMFAC for the variable composition of each individual phase. Furthermore, the solid-liquid equilibrium of crystalline AS with AS dissolved in an aqueous (sucrose-rich) phase was also solved numerically based on the method described in Hodas et al. (2016).<sup>52</sup> The molar input concentrations were determined using the mole fractions of sucrose and AS in the dry particles, and the RH values at which each particle was equilibrated before exposure to DMA were used to specify the initial mixture composition. The equilibrium computations were carried out for a constant temperature of 297.15 K, representative of the experimental conditions. The AIOMFAC-based LLE model predictions for the equilibrium-phase compositions of liquid particle phases  $\alpha$ and  $\beta$ , and solid AS phase  $\delta$  (where applicable), as well as associated component activity coefficients were then used as input parameters to constrain the kinetic model simulations with KM-GAP.

**Field Measurements.** We analyzed particle- and gas-phase concentrations of ammonia and amines measured during the Holistic Interactions of Shallow Clouds, Aerosols and Land Ecosystems (HI-SCALE) field campaign in north-central Oklahoma in the summer of 2016. Gas-phase amines were measured by ambient-pressure proton transfer mass spectrometry. Concomitant measurements of size-resolved nanoparticle composition were performed during HI-SCALE by Thermal Desorption Chemical Ionization Mass Spectrometry (TDCIMS). Calibrations were performed during the campaign using either atomized AS or DMAS particles to associate signal intensity to collected sample mass. The average RH measured during this campaign was  $72 \pm 18\%$  ( $1\sigma$ ), with peaks in RH at night.

## ■ RESULTS AND DISCUSSION

Pure Ammonium Sulfate Particles. Figure 2a shows experimental data from Chu and Chan (2017)<sup>18</sup> and modeled particle mass ratio for the pure AS particles as a function of exposure time to DMA. The particle mass ratio is defined as the mass of the particle at time t relative to that at time 0  $(t_0)$ . The particle mass ratio increases both due to conversion of AS to DMAS and the increase in associated water content of the particle. Particle mass ratios increase at different rates depending on RH until they reach a plateau at the completion of the DMA/ammonium displacement reaction. The rate of particle growth was fastest for the aqueous particle at 70% RH, and sensitivity studies revealed that, for this condition, growth is limited only by gas-phase diffusion of DMA.<sup>56</sup> The bulk diffusion coefficients of DMA increase as RH increases, leading to higher rates of reaction and particle growth rates. The model simulations reveal that predicted mass ratios are sensitive to the Henry's law coefficient, the bulk diffusion coefficient of DMA, and the initial concentration of AS in the surface layer. Therefore, the availability of DMA and AS in the surface layer during the initial stages of DMA uptake controls the rate of particle growth. At 30% RH the particle mass ratio reaches a plateau at a high value, as the particle undergoes a phase transition from solid to liquid due to DMAS formation and associated water uptake. This phase transition leads to an enhancement in the liquid particle mass relative to the dry mass at time zero, which is different from the case at 70% RH, in which no phase transition occurs. Chu and Chan (2017)<sup>18</sup> observed that the particle phase gradually transformed from crystalline solid into liquid during DMA uptake judging from the 90° Mie scattering pattern and Raman spectrum of the particle.

The temporal evolution of concentration of each component over time in the surface layer is shown in Figure 3. While a

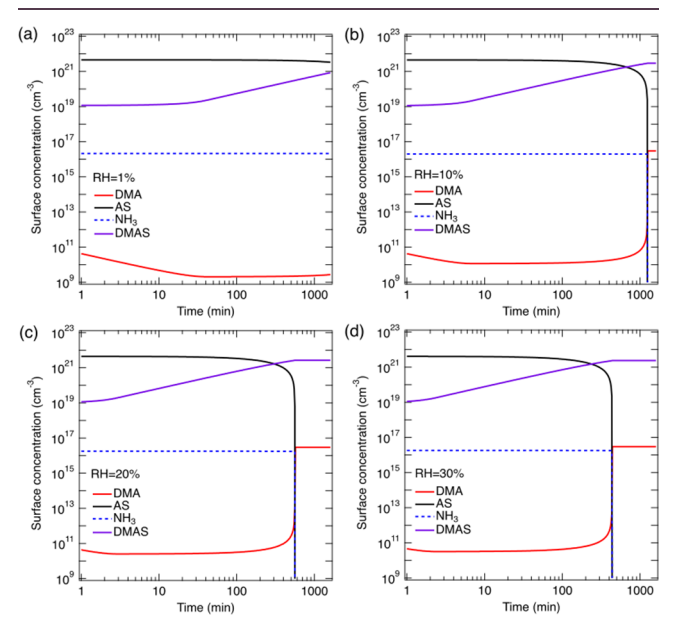


**Figure 3.** Predicted concentrations (molecules per cm<sup>3</sup>) using KM-GAP for DMA (red), AS (black), NH<sub>3</sub>(dashed blue) and DMAS (purple) in the surface layer during DMA uptake by an AS particle at RH of (a) 1%, (b) 10%, (c) 20%, and (d) 30%.

minimal decrease in AS concentration is observed for RH < 5% (Figure 3a), the reaction proceeds to completion at all other RH values and the AS concentration drops to zero as the DMAS concentration plateaus. A drop in DMA concentration (red line) may be observed while the exchange reaction proceeds due to the volume of the surface layer growing, while the rate of DMA accommodation to this layer remains relatively constant. Once the reaction reaches completion in Figures 3b-d, the DMA concentration begins to increase until it reaches the saturation concentration. The concentration of NH $_3$  in the surface layer (dotted blue line) remains constant while the reaction is occurring as determined by the balance between formation and evaporation but drops to zero due to particle-to-gas partitioning once the reaction has reached completion.

The temporal evolution of bulk concentration profiles of components for the aqueous particle at 70% RH is provided in Figure 4 as a function of reaction time (x-axis) and distance from the particle center (y-axis). The concentration of AS (Figure 4a) decreases commensurate with an increase in the

concentration of DMAS (Figure 4b). Since the particle is initially aqueous, all AS is dissolved, and no diffusion limitation is observed. A low concentration of DMA is present until the reaction reaches completion, as DMA diffusing into the particle bulk is rapidly consumed by the exchange (Figure 4c). The concentration of NH<sub>3</sub> (Figure 4d) in the particle is constant until the reaction completes. It then drops due to particle-togas partitioning, as observed in the surface layer.

Mixed Ammonium Sulfate-Sucrose Particles. Figure 5 shows the mass fractions of the components in the AS/ sucrose/water system at time zero as predicted by the AIOMFAC-LLE model for the case with a dry molar sucrose fraction of  $F_{Su}$  = 0.15. Thermodynamic equilibrium computations were conducted for both dehydration and hydration cases. In the dehydration case starting from high RH conditions with all components in a liquid/amorphous phase, a metastable, supersaturated salt solution is considered and crystallization suppressed in the calculations (Figure 5b), while in the hydration case, starting at low RH, AS is allowed to adopt a crystalline physical state below its predicted complete deliquescence at ~79% RH (Figure 5a). In the hydration case, AS is predominantly partitioned to the solid phase  $(\delta)$ , while sucrose is found in a separate amorphous/liquid phase that further contains water and small amounts of dissolved AS (in solid-liquid equilibrium) up to the complete AS deliquescence at  $\sim$ 79% RH. Two liquid phases, one AS-rich ( $\alpha$ ) and one sucrose-rich ( $\beta$ ), are predicted to coexist between 79% < RH < 94% in the hydration case. For the dehydration case, liquidliquid phase separation leads to the formation of AS-rich ( $\alpha$ ) and sucrose-rich ( $\beta$ ) phases at RH < 94% (before AS is expected to crystallize spontaneously at RH ≤ 36%, not shown in Figure 5b). In the phase-separated regime, a non-negligible fraction of AS is predicted to partition into the sucrose-rich (aqueous) phase, while the aqueous AS-rich phase  $\alpha$  is virtually sucrose-free, except for the RH range from ~84% to 93%, close to the upper limit of phase separation, in which at least 1% of the total sucrose amount partitions into phase  $\alpha$ .

These predicted compositions were used to constrain the initial partitioning of components in KM-GAP. Based on experimental data on aerosol morphologies, <sup>18</sup> KM-GAP treats the AS-rich phase as the core and the sucrose-rich phase as the shell (Figure 1b), and the predicted activity coefficients of the different species in each phase were used to constrain bulk diffusion. For RH < 70%, values from the hydration branch (Figure 5a) were used, while activity coefficients from the dehydration branch (Figure 5b) were used for 70% RH. We assume that liquid-liquid phase separation persisted at 70% RH while the reaction occurred and ammonium ions were replaced by aminium ions, since the AIOMFAC model predicted that phase separation is more strongly driven by the sulfate ions interacting with the organics. It should be noted, however, that some of the particles at RH < 70% were observed to remain amorphous and water-bound in the experiment. The predicted equilibrium thicknesses of the sucrose-rich phase at different RH values will depend on the dry particle diameter considered. Thermodynamic modeling of layer thickness was conducted with AIOMFAC using the dehydration case where there is no solid AS phase (Figure 5b). The change in radius as a function of RH for a 40  $\mu$ m diameter particle with  $F_{Su} = 0.15$  is provided in Figure S1a. At 40% RH, the sucrose-rich shell thickness is  $\sim$ 13% of the total radius. At 80% RH, the shell thickness is ~10% of the total radius. The thickness of the shell increases with increasing  $F_{Su}$ . Our kinetic

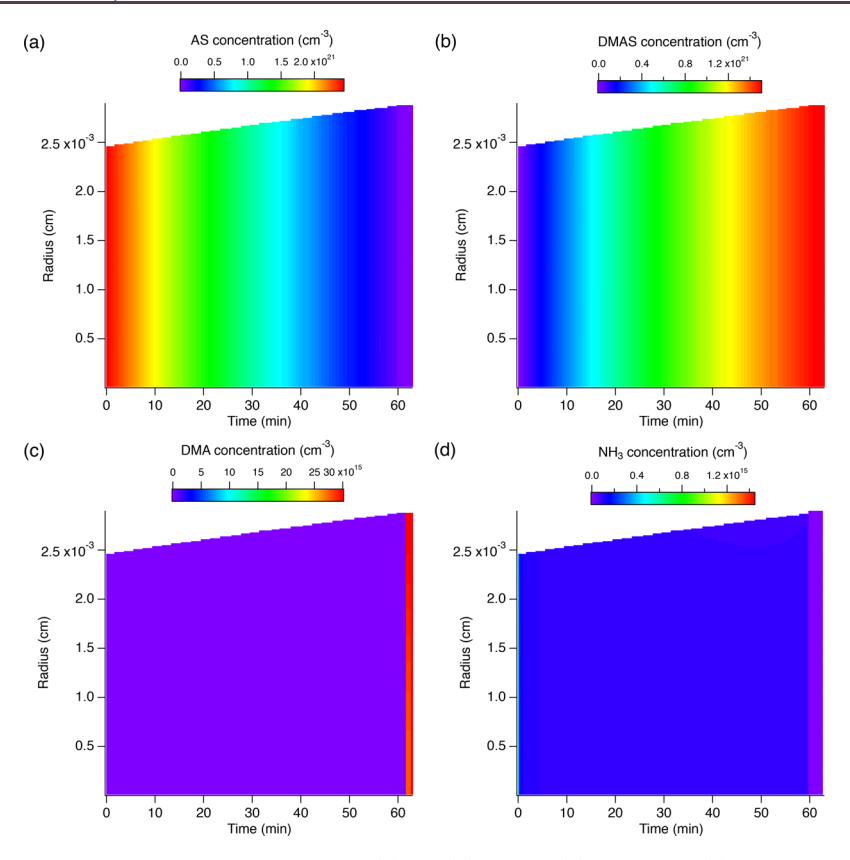


Figure 4. Predicted bulk concentration profiles using KM-GAP for (a) AS, (b) DMAS, (c) DMA, and (d) NH<sub>3</sub> when an AS particle is exposed to DMA at 70% RH.

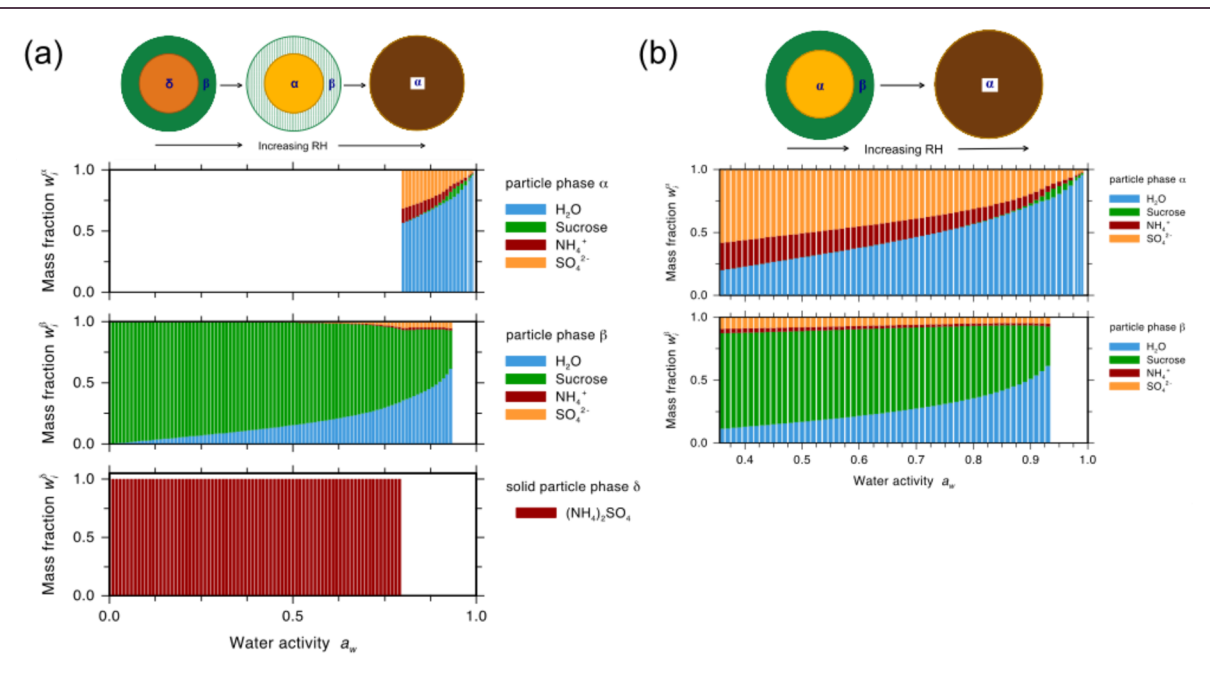
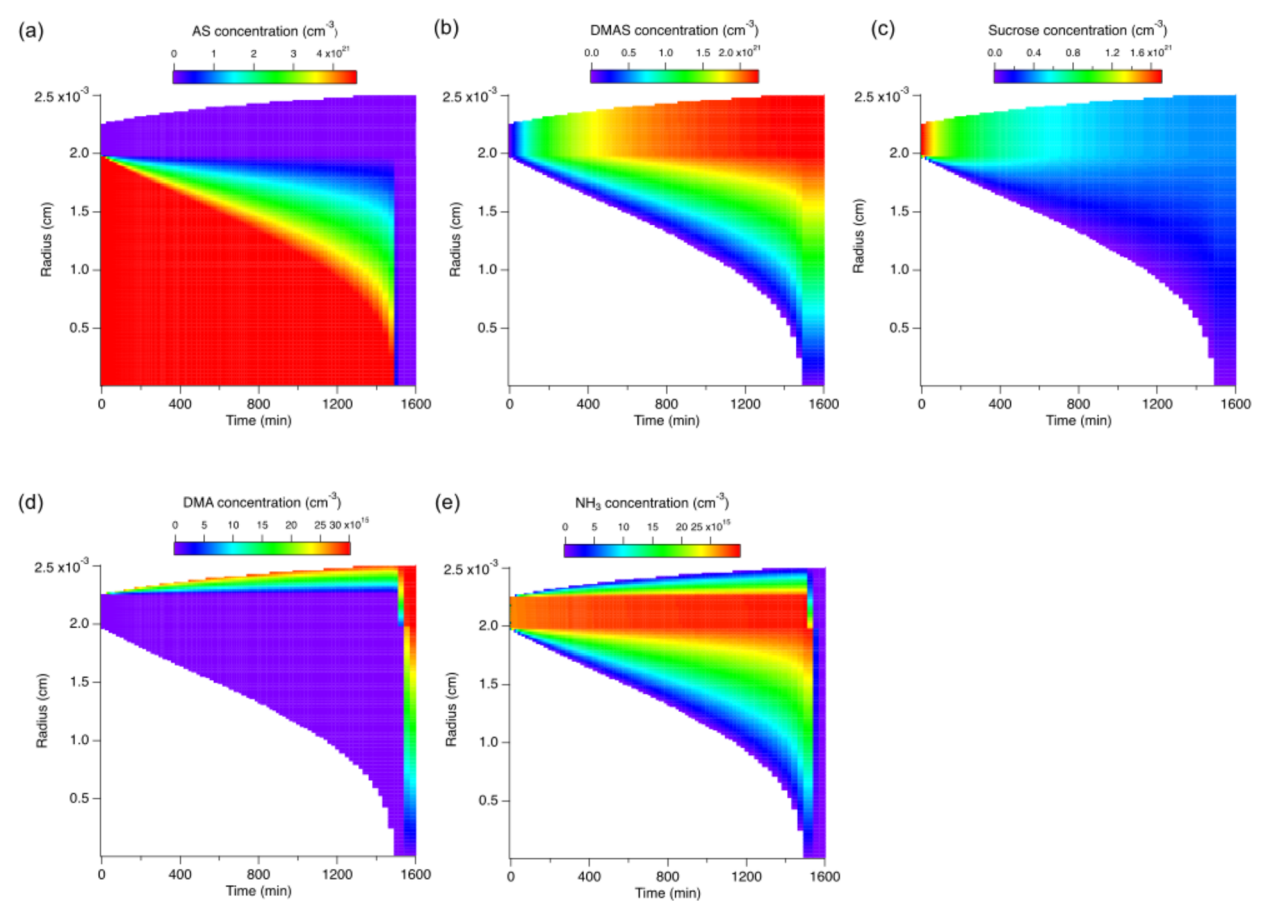


Figure 5. Predicted equilibrium-phase compositions in mass fractions for aqueous mixtures of AS and sucrose as a function of water activity (equilibrium RH) at 297.15 K. (a) Hydration case: a solid–liquid equilibrium is predicted between a solid AS phase ( $\delta$ ; lowest panel) and an aqueous, sucrose-rich phase ( $\beta$ ; middle panel) up to 70% RH, followed by liquid–liquid phase separation (coexisting phases  $\alpha$  and  $\beta$ ) and merging into a single liquid phase at RH > 93%. (b) In the dehydration case, formation of solid AS is suppressed, extending the liquid–liquid phase separation range to lower RH, with both phases becoming AS-supersaturated below 79% RH.

model utilizes the initial number of molecules in a layer to determine its thickness. The thickness of the sucrose shell used in the KM-GAP model for each experiment is listed in Table S3. As can be seen in Figure 6, the initial thickness of the

sucrose-rich shell is approximately 2.5  $\mu$ m, with a core radius of  $\sim$ 20  $\mu$ m.

Figure 2b-d shows the experimental measurements and KM-GAP modeling results for the mixed AS-sucrose particles.



**Figure 6.** Concentration (molecules per cm<sup>3</sup>) of components in the core and shell of the particle (at  $F_{Su} = 0.15$ , RH = 10%) as a function of time (x-axis) and distance from the particle center (y-axis): (a) AS, (b) DMAS, (c) sucrose, (d) DMA, and (e) NH<sub>3</sub>. Color bar indicates concentration (molecules cm<sup>-3</sup>), with red indicating areas of high concentration and blue indicating low concentration.

Table 3. Modeled True and Effective (in Parentheses) Uptake Coefficients ( $\gamma$ ) for Dimethylamine

	relative humidity (%)						
$F_{ m Su}$	1	10	20	30	70		
0.00	$7.75 \times 10^{-5} $ $(7.59 \times 10^{-5})$	$3.87 \times 10^{-4}$ $(3.54 \times 10^{-4})$	$9.27 \times 10^{-4}$ $(7.68 \times 10^{-4})$	$9.28 \times 10^{-4}$ $(7.86 \times 10^{-4})$	$0.82 \\ (4.18 \times 10^{-3})$		
0.15	$3.41 \times 10^{-5} $ $(3.38 \times 10^{-5})$	$3.87 \times 10^{-4}$ $(3.57 \times 10^{-4})$	$1.23 \times 10^{-3}$ $(0.95 \times 10^{-3})$	$2.54 \times 10^{-3}$ $(1.27 \times 10^{-3})$	$0.80 \\ (3.47 \times 10^{-3})$		
0.28	$2.74 \times 10^{-5}$ $(2.71 \times 10^{-5})$	$2.05 \times 10^{-4}$ $(1.97 \times 10^{-4})$	$7.08 \times 10^{-4}$ $(7.08 \times 10^{-4})$	(a) $2.60 \times 10^{-3}$ $(1.64 \times 10^{-3})$ (b) $2.19 \times 10^{-3}$ $(1.37 \times 10^{-3})$	$0.75 \\ (4.13 \times 10^{-3})$		
0.50	$1.42 \times 10^{-7}$ $(1.42 \times 10^{-7})$	$1.00 \times 10^{-6}$ $(1.00 \times 10^{-6})$	$2.78 \times 10^{-4}$ $(2.64 \times 10^{-4})$	$9.84 \times 10^{-4}$ $(8.18 \times 10^{-4})$	$0.70 \\ (3.61 \times 10^{-3})$		

The particle growth of aqueous mixed particles at 70% RH at all mole fractions of sucrose was limited by gas-phase diffusion. For RH < 70%, the mixed AS-sucrose particles differed from the pure AS particles in that the mixed particles exhibited no sensitivity to the value of the Henry's law coefficient. Instead, the growth of the mixed particles is limited only by the bulk diffusion coefficients of DMA and AS through the sucrose-rich shell.

Figure 6 shows bulk concentration profiles of the model components for the particle with  $F_{Su} = 0.15$  at 10% RH. The

concentration of AS in the sucrose-rich particle shell (Figure 6a) remains low due to slow transport of AS from the AS-rich core to the sucrose-rich shell and loss by the displacement reaction. As the reaction progresses and the particle grows, the AS core decreases in size and the shell volume increases, as exhibited by the plots of DMAS, sucrose, and ammonia concentration (Figure 6b, c, e, respectively). The reaction products (e.g., DMAS, NH<sub>3</sub>) are mostly concentrated in the outer portion of the particle shell throughout the reaction. Sucrose does not react with DMA, so the number of sucrose

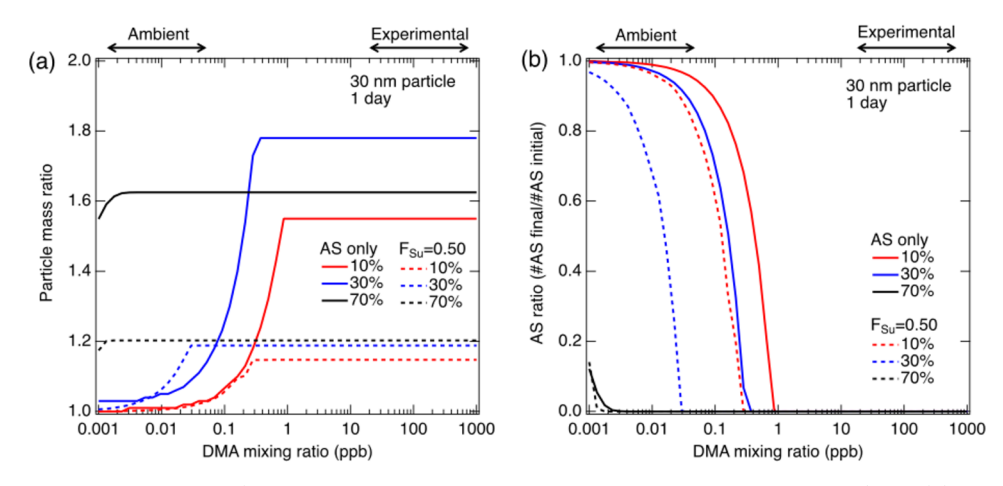


Figure 7. (a) Predicted particle mass ratios (particle mass after exposure to DMA divided by initial particle mass) and (b) molar AS ratio (number of AS molecules after DMA exposure divided by initial number of AS molecules) as a function of DMA mixing ratio. Kinetic modeling was used to simulate DMA uptake by pure AS or AS-sucrose ( $F_{su} = 0.50$ ) particles with 30 nm diameter over 1 day at varying DMA mixing ratios. DMA mixing ratios range from ppt levels found in the atmosphere to ppm levels used in experimental data. A reaction rate coefficient of  $1 \times 10^{-15}$  cm<sup>3</sup> s<sup>-1</sup> was used for the simulations.

molecules does not change as the reaction proceeds, and the molecular concentration of sucrose decreases due to dilution as the shell volume grows. The concentration of DMA is highest near the surface of the particle, before it encounters AS as it diffuses into the shell. Similar trends in bulk concentration were observed for other mixed AS-sucrose particles for which the exchange reaction reached completion.

The reaction reaches completion over the experimental time period for all conditions apart from RH < 5% and 10% RH when  $F_{Su}$  = 0.50. With  $F_{Su}$  = 0.50 at 10% RH, the increase in particle mass ratio is severely diminished and becomes almost indistinguishable from the RH < 5% case due to strong kinetic limitations of bulk diffusion (with bulk diffusivity <5.0 × 10<sup>-13</sup> cm<sup>2</sup> s<sup>-1</sup>) in a glassy sucrose-rich shell.

Further indications of kinetic limitations can be found by comparing values of the uptake coefficient for each particle. DMA uptake coefficients (the ratio between net uptake rates to molecular collision rates) calculated from the model are summarized in Table 3, which also includes effective uptake coefficients which are calculated without considering gas-phase diffusion (i.e., collision rates were calculated using average gasphase concentrations). A large difference between the true and effective uptake coefficients at 70% RH demonstrates the importance of gas-phase diffusion at high RH, where nearsurface gas-phase concentrations are reduced due to large uptake. The order of magnitude values for the effective uptake coefficients (Table 3) are consistent with those derived from laboratory experiments, with the largest discrepancy within 1 order of magnitude. 18 DMA uptake coefficients range from 7.8  $\times$  10<sup>-5</sup> to 2.6  $\times$  10<sup>-3</sup> for initially solid particles at RH < 70%, while they are 0.70-0.82 for initially aqueous particles at 70% RH.

The modeled uptake coefficients follow similar trends as the reported, experimentally derived values: DMA uptake increases as RH increases for all molar fractions of sucrose. An examination of AS concentrations in the modeled particles reveals that the concentration of AS in the shell increases with increasing RH. The higher AS concentration is consistent with increased solvation of AS with higher water content (as shown in Figure 5), resulting in higher DMA uptake. In general uptake coefficients decrease as the molar fraction of sucrose

increases. The plausible explanation for the effect of sucrose is a change in viscosity of the shell layer. The higher viscosity of sucrose-containing aqueous solutions at intermediate and low RH is well-documented.<sup>57</sup> As the relative amount of sucrose in the particle increases, the higher viscosity of the sucrose-rich layers would affect bulk diffusion of DMA.

Atmospheric Implications and Conclusion. Using the kinetic model, we sought to extrapolate to particle sizes and DMA mixing ratios representative of ambient conditions to assess atmospheric implications. The experiments conducted by Chu and Chan  $(2017)^{18}$  were performed on particles with diameters in the micrometer range (37-71 mm) at a DMA mixing ratio of 1 ppm. Analysis of particle and gas-phase concentrations of ammonia and amines measured during the HI-SCALE field campaign in north-central Oklahoma in the summer of 2016 provided values for use as reference. The average mixing ratios of ammonia, DMA, and methylamine were  $245 \pm 47$  ppt,  $0.813 \pm 0.670$  ppt, and  $0.601 \pm 0.480$  ppt, respectively. TDCIMS measurements detected particulate ammonium and aminium salts in 20-40 nm particles.

Given this information, we simulated the growth of a 30 nm AS particle over 1 day upon exposure to DMA at mixing ratios varying from typical levels of 1 ppm in laboratory experiments to the 1 ppt range observed in the HI-SCALE field measurements. The predicted mass ratios as a function of DMA mixing ratio are shown in Figure 7a. Also included is the predicted ratio of remaining AS to initial AS for the same conditions (Figure 7b). Unlike the simulations corresponding to the experimental data, for the significantly smaller atmospherically relevant particle sizes, DMA uptake is sensitive to the reaction rate coefficient as shown by sensitivity tests in Figures S2-S5. Growth is likely to be limited for atmospherically relevant DMA mixing ratios at lower RH values (Figures 7, S2, and S4). However, in the presence of hydrophilic organics and with a high reaction rate coefficient ( $\sim 10^{-13}$  cm<sup>3</sup> s<sup>-1</sup>), substantial growth would occur (Figure S4). Significant growth is predicted at 70% RH under atmospheric conditions (Figures 7, S3, and S5) unless the rate coefficient is low  $(\sim 10^{-17} \text{ cm}^3 \text{ s}^{-1})$ . For the 30 nm particles used for these simulations, the increase in mass ratio is no longer limited by gas-phase diffusion at 70% RH; therefore, if we assume a fast

reaction rate, the reaction proceeds quickly and reaches completion after 1 day, even at low DMA mixing ratios. 58 This observation also applies to the mixed AS-sucrose particles modeled at a sucrose mole fraction of  $F_{Su} = 0.50$ . Thermodynamic modeling of layer thickness was also conducted with AIOMFAC for a 30 nm particle with liquid-liquid phase separation ( $\alpha$  and  $\beta$  phases). Results are provided in Figure S1b and are similar in proportion to those for the larger particles. These results suggest that, in locations of high RH, when aerosol particles are in the liquid-phase state, amine uptake could result in a mass increase by approximately 20-60%, depending on the composition of the particle. However, given the sensitivity of the kinetic model to the reaction rate constant at ambient conditions, measurements of smaller particles are needed to better constrain the reaction rate coefficient in the model.

Further work on smaller particles is required to fully understand the importance of aminium formation on particle growth. Another important factor to consider is the Kelvin effect, which becomes important for small particles. The liquid—liquid phase separation as a phenomenon is assumed to be approximately unchanged by the particle size at the 30 nm scale, but the separation relative humidity (SRH) would potentially need to be adjusted for the competing effects of the Kelvin effect and liquid—liquid interfacial energy, each acting in a different direction in terms of increasing/decreasing SRH.<sup>59</sup> The kinetic model described in this paper was motivated by experimental work on simplified mixed particles containing only AS and one organic compound. In contrast, TDCIMS measurements of particulate ammonium in 20-40 nm particles during HI-SCALE found that ~47 wt% of the detected ammonium can be attributed to AS, suggesting that other counterions for ammonium exist in particles such as nitrate or deprotonated organic acids. TDCIMS measurements also determined that amine salts could be important constituents of ambient particles. Applying the assumption that the measured DMA and methylamine form neutralized salts with sulfuric acid, HI-SCALE measurements determined that DMA sulfate comprises 20.0 ± 36.8 wt% (uncertainties here indicate standard deviation and not measurement uncertainty) and methylaminium sulfate comprises 20.1 ± 38.1 wt% of 20-40 nm particles, although it is also likely that these strong bases form salts with other particulate anions. These findings from HI-SCALE are consistent with previous field measurements in which 10-47% of TDCIMS-detected positive ions were attributed to aminium salts depending on location.4 Thus, while the amine/ammonium exchange reaction could contribute to formation of ambient particles, HI-SCALE measurements suggest other ammonium salts are also present in ambient particles and must be considered in future investigations.

It should also be noted that all experiments were conducted at a temperature near 298 K. Seasonal fluctuations lead to lower and higher temperatures throughout the world. At lower temperatures, viscosity will increase so particles are expected to become more viscous and kinetic limitations are more likely for DMA uptake, whereas kinetic limitations are not expected at higher temperatures. In addition, geographic location and atmospheric altitude are important as SOA are predicted to be liquid in regions of high RH, semi-solid in the mid-latitude areas and solid over dry lands, and in the middle and upper troposphere.

#### ASSOCIATED CONTENT

# S Supporting Information

The Supporting Information is available free of charge on the ACS Publications website at DOI: 10.1021/acsearthspace-chem.9b00142.

Dependence of phase thickness on RH; sensitivity of particle mass ratio to DMA concentration; general parameters used for KM-GAP; input parameters for AS-only particles; input parameters for mixed AS-sucrose particles, including Figures S1–S5 and Tables S1–S3 (PDF)

#### AUTHOR INFORMATION

## **Corresponding Author**

\*E-mail: m.shiraiwa@uci.edu.

#### ORCID (

Yangxi Chu: 0000-0003-0204-0025 Chak K. Chan: 0000-0001-9687-8771 James N. Smith: 0000-0003-4677-8224 Manabu Shiraiwa: 0000-0003-2532-5373

#### **Author Contributions**

<sup>1</sup>W.-S.W.D. and P.S.J.L. contributed equally to this work.

#### Notes

The authors declare no competing financial interest.

#### ACKNOWLEDGMENTS

This work was funded by the National Science Foundation (AGS-1654104) and the Department of Energy (DE-SC0018349 and DE-SC0019000).

# **■** REFERENCES

- (1) Finlayson-Pitts, B. J.; Pitts, J. N. Tropospheric air pollution: ozone, airborne toxics, polycyclic aromatic hydrocarbons, and particles. *Science* **1997**, 276 (5315), 1045–1051.
- (2) Pöschl, U.; Shiraiwa, M. Multiphase chemistry at the atmosphere-biosphere interface influencing climate and public health in the anthropocene. *Chem. Rev.* **2015**, *115* (10), 4440–4475.
- (3) Ravishankara, A. R.; Rudich, Y.; Wuebbles, D. J. Physical chemistry of climate metrics. *Chem. Rev.* **2015**, *115* (10), 3682–3703.
- (4) Smith, J. N.; Barsanti, K. C.; Friedli, H. R.; Ehn, M.; Kulmala, M.; Collins, D. R.; Scheckman, J. H.; Williams, B. J.; McMurry, P. H. Observations of aminium salts in atmospheric nanoparticles and possible climatic implications. *Proc. Natl. Acad. Sci. U. S. A.* **2010**, *107* (15), 6634–6639.
- (5) Silvern, R. F.; Jacob, D. J.; Kim, P. S.; Marais, E. A.; Turner, J. R.; Campuzano-Jost, P.; Jimenez, J. L. Inconsistency of ammonium-sulfate aerosol ratios with thermodynamic models in the eastern US: a possible role of organic aerosol. *Atmos. Chem. Phys.* **2017**, *17* (8), 5107–5118.
- (6) Arquero, K. D.; Xu, J.; Gerber, R. B.; Finlayson-Pitts, B. J. Particle formation and growth from oxalic acid, methanesulfonic acid, trimethylamine and water: a combined experimental and theoretical study. *Phys. Chem. Chem. Phys.* **2017**, *19* (41), 28286–28301.
- (7) Rovelli, G.; Miles, R. E. H.; Reid, J. P.; Clegg, S. L. Hygroscopic properties of aminium sulfate aerosols. *Atmos. Chem. Phys.* **2017**, *17* (6), 4369–4385.
- (8) Angelino, S.; Suess, D. T.; Prather, K. A. Formation of aerosol particles from reactions of secondary and tertiary alkylamines: Characterization by aerosol time-of-flight mass spectrometry. *Environ. Sci. Technol.* **2001**, *35* (15), 3130–3138.
- (9) Facchini, M. C.; Decesari, S.; Rinaldi, M.; Carbone, C.; Finessi, E.; Mircea, M.; Fuzzi, S.; Moretti, F.; Tagliavini, E.; Ceburnis, D.; O'Dowd, C. D. Important source of marine secondary organic aerosol

- from biogenic amines. Environ. Sci. Technol. 2008, 42 (24), 9116–9121.
- (10) Pratt, K. A.; Hatch, L. E.; Prather, K. A. Seasonal volatility dependence of ambient particle phase amines. *Environ. Sci. Technol.* **2009**, 43 (14), 5276–5281.
- (11) Sorooshian, A.; Murphy, S.; Hersey, S.; Gates, H.; Padro, L.; Nenes, A.; Brechtel, F.; Jonsson, H.; Flagan, R.; Seinfeld, J. Comprehensive airborne characterization of aerosol from a major bovine source. *Atmos. Chem. Phys.* **2008**, *8* (17), 5489–5520.
- (12) Ge, X.; Wexler, A. S.; Clegg, S. L. Atmospheric amines Part I. A review. *Atmos. Environ.* **2011**, *45* (3), 524–546.
- (13) Qiu, C.; Wang, L.; Lal, V.; Khalizov, A. F.; Zhang, R. Heterogeneous reactions of alkylamines with ammonium sulfate and ammonium bisulfate. *Environ. Sci. Technol.* **2011**, 45 (11), 4748–4755.
- (14) Liu, Y.; Han, C.; Liu, C.; Ma, J.; Ma, Q.; He, H. Differences in the reactivity of ammonium salts with methylamine. *Atmos. Chem. Phys.* **2012**, *12* (11), 4855–4865.
- (15) Sauerwein, M.; Chan, C. K. Heterogeneous uptake of ammonia and dimethylamine into sulfuric and oxalic acid particles. *Atmos. Chem. Phys.* **2017**, *17* (10), 6323–6339.
- (16) Chan, L. P.; Chan, C. K. Displacement of ammonium from aerosol particles by uptake of triethylamine. *Aerosol Sci. Technol.* **2012**, 46 (2), 236–247.
- (17) Chu, Y.; Chan, C. K. Role of oleic acid coating in the heterogeneous uptake of dimethylamine by ammonium sulfate particles. *Aerosol Sci. Technol.* **2017**, *51* (8), 988–997.
- (18) Chu, Y.; Chan, C. K. Reactive uptake of dimethylamine by ammonium sulfate and ammonium sulfate-sucrose mixed particles. *J. Phys. Chem. A* **2017**, *121* (1), 206–215.
- (19) Reid, J. P.; Bertram, A. K.; Topping, D. O.; Laskin, A.; Martin, S. T.; Petters, M. D.; Pope, F. D.; Rovelli, G. The viscosity of atmospherically relevant organic particles. *Nat. Commun.* **2018**, *9* (1), 956
- (20) De Rieux, W.-S.; Li, Y.; Lin, P.; Laskin, J.; Laskin, A.; Bertram, A. K.; Nizkorodov, S. A.; Shiraiwa, M. Predicting the glass transition temperature and viscosity of secondary organic material using molecular composition. *Atmos. Chem. Phys.* **2018**, *18* (9), 6331–6351.
- (21) Koop, T.; Bookhold, J.; Shiraiwa, M.; Poeschl, U. Glass transition and phase state of organic compounds: dependency on molecular properties and implications for secondary organic aerosols in the atmosphere. *Phys. Chem. Chem. Phys.* **2011**, *13* (43), 19238–19255
- (22) Virtanen, A.; Joutsensaari, J.; Koop, T.; Kannosto, J.; YliPirilä, P.; Leskinen, J.; Mäkelä, J. M.; Holopainen, J. K.; Pöschl, U.; Kulmala, M.; Worsnop, D. R.; Laaksonen, A. An amorphous solid state of biogenic secondary organic aerosol particles. *Nature* **2010**, *467*, 824–827.
- (23) Renbaum-Wolff, L.; Grayson, J. W.; Bateman, A. P.; Kuwata, M.; Sellier, M.; Murray, B. J.; Shilling, J. E.; Martin, S. T.; Bertram, A. K. Viscosity of  $\alpha$ -pinene secondary organic material and implications for particle growth and reactivity. *Proc. Natl. Acad. Sci. U. S. A.* **2013**, *110* (20), 8014–8019.
- (24) Knopf, D. A.; Alpert, P. A.; Wang, B. The Role of organic aerosol in atmospheric ice nucleation: a review. ACS Earth Space Chem. 2018, 2 (3), 168–202.
- (25) Li, Y.; Shiraiwa, M. Timescales of secondary organic aerosols to reach equilibrium at various temperatures and relative humidities. *Atmos. Chem. Phys.* **2019**, *19* (9), 5959–5971.
- (26) Shiraiwa, M.; Ammann, M.; Koop, T.; Pöschl, U. Gas uptake and chemical aging of semisolid organic aerosol particles. *Proc. Natl. Acad. Sci. U. S. A.* **2011**, *108* (27), 11003–11008.
- (27) Berkemeier, T.; Steimer, S. S.; Krieger, U. K.; Peter, T.; Poschl, U.; Ammann, M.; Shiraiwa, M. Ozone uptake on glassy, semi-solid and liquid organic matter and the role of reactive oxygen intermediates in atmospheric aerosol chemistry. *Phys. Chem. Chem. Phys.* **2016**, *18* (18), 12662–74.
- (28) Marshall, F. H.; Miles, R. E.; Song, Y.-C.; Ohm, P. B.; Power, R. M.; Reid, J. P.; Dutcher, C. S. Diffusion and reactivity in ultraviscous

- aerosol and the correlation with particle viscosity. *Chem. Sci.* **2016**, *7*, 1298–1308.
- (29) Arangio, A. M.; Slade, J. H.; Berkemeier, T.; Pöschl, U.; Knopf, D. A.; Shiraiwa, M. Multiphase chemical kinetics of OH radical uptake by molecular organic markers of biomass burning aerosols: humidity and temperature dependence, surface reaction, and bulk diffusion. *J. Phys. Chem. A* **2015**, *119* (19), 4533–4544.
- (30) Slade, J. H.; Knopf, D. A. Multiphase OH oxidation kinetics of organic aerosol: The role of particle phase state and relative humidity. *Geophys. Res. Lett.* **2014**, *41* (14), 5297–5306.
- (31) Wiegel, A. A.; Liu, M. J.; Hinsberg, W. D.; Wilson, K. R.; Houle, F. A. Diffusive confinement of free radical intermediates in the OH radical oxidation of semisolid aerosols. *Phys. Chem. Chem. Phys.* **2017**, 19 (9), 6814–6830.
- (32) Lakey, P. S. J.; Berkemeier, T.; Krapf, M.; Dommen, J.; Steimer, S. S.; Whalley, L. K.; Ingham, T.; Baeza-Romero, M. T.; Poschl, U.; Shiraiwa, M.; Ammann, M.; Heard, D. E. The effect of viscosity and diffusion on the HO<sub>2</sub> uptake by sucrose and secondary organic aerosol particles. *Atmos. Chem. Phys.* **2016**, *16* (20), 13035–13047.
- (33) You, Y.; Smith, M. L.; Song, M.; Martin, S. T.; Bertram, A. K. Liquid-liquid phase separation in atmospherically relevant particles consisting of organic species and inorganic salts. *Int. Rev. Phys. Chem.* **2014**, 33 (1), 43–77.
- (34) Freedman, M. A. Phase separation in organic aerosol. *Chem. Soc. Rev.* **2017**, *46* (24), 7694–7705.
- (35) Gorkowski, K.; Donahue, N. M.; Sullivan, R. C. Emerging investigator series: determination of biphasic core-shell droplet properties using aerosol optical tweezers. *Environ. Sci.: Processes Impacts* **2018**, 20 (11), 1512–1523.
- (36) Song, M.; Liu, P.; Martin, S. T.; Bertram, A. K. Liquid-liquid phase separation in particles containing secondary organic material free of inorganic salts. *Atmos. Chem. Phys.* **2017**, *17* (18), 11261–11271.
- (37) Pöhlker, C.; Wiedemann, K. T.; Sinha, B.; Shiraiwa, M.; Gunthe, S. S.; Smith, M.; Su, H.; Artaxo, P.; Chen, Q.; Cheng, Y.; Elbert, W.; Gilles, M. K.; Kilcoyne, A. L. D.; Moffet, R. C.; Weigand, M.; Martin, S. T.; Pöschl, U.; Andreae, M. O. Biogenic potassium salt particles as seeds for secondary organic aerosol in the Amazon. *Science* **2012**, 337 (6098), 1075–1078.
- (38) Riemer, N.; Ault, A. P.; West, M.; Craig, R. L.; Curtis, J. H. Aerosol mixing state: measurements, modeling, and impacts. *Rev. Geophys.* **2019**, *57*, 1–63.
- (39) Krieger, U. K.; Marcolli, C.; Reid, J. P. Exploring the complexity of aerosol particle properties and processes using single particle techniques. *Chem. Soc. Rev.* **2012**, *41* (19), 6631–6662.
- (40) Zhang, Y.; Chen, Y.; Lambe, A. T.; Olson, N. E.; Lei, Z.; Craig, R. L.; Zhang, Z.; Gold, A.; Onasch, T. B.; Jayne, J. T.; Worsnop, D. R.; Gaston, C. J.; Thornton, J. A.; Vizuete, W.; Ault, A. P.; Surratt, J. D. Effect of the aerosol-phase state on secondary organic aerosol formation from the reactive uptake of isoprene-derived epoxydiols (IEPOX). *Environ. Sci. Technol. Lett.* 2018, 5 (3), 167–174.
- (41) Vander Wall, A. C.; Lakey, P. S. J.; Rossich Molina, E.; Perraud, V.; Wingen, L. M.; Xu, J.; Soulsby, D.; Gerber, R. B.; Shiraiwa, M.; Finlayson-Pitts, B. J. Understanding interactions of organic nitrates with the surface and bulk of organic films: implications for particle growth in the atmosphere. *Environ. Sci. Processes Impacts* **2018**, *20* (11), 1593–1610.
- (42) Gorkowski, K.; Donahue, N. M.; Sullivan, R. C. Emulsified and liquid-liquid phase-separated states of  $\alpha$ -pinene secondary organic aerosol determined using aerosol optical tweezers. *Environ. Sci. Technol.* **2017**, *51* (21), 12154–12163.
- (43) Shiraiwa, M.; Pfrang, C.; Koop, T.; Poeschl, U. Kinetic multilayer model of gas-particle interactions in aerosols and clouds (KM-GAP): linking condensation, evaporation and chemical reactions of organics, oxidants and water. *Atmos. Chem. Phys.* **2012**, *12* (5), 2777–2794.
- (44) Mikhailov, E.; Vlasenko, S.; Martin, S. T.; Koop, T.; Poeschl, U. Amorphous and crystalline aerosol particles interacting with water vapor: conceptual framework and experimental evidence for

- restructuring, phase transitions and kinetic limitations. *Atmos. Chem. Phys.* **2009**, 9 (24), 9491–9522.
- (45) Zuend, A.; Marcolli, C.; Booth, A. M.; Lienhard, D. M.; Soonsin, V.; Krieger, U. K.; Topping, D. O.; McFiggans, G.; Peter, T.; Seinfeld, J. H. New and extended parameterization of the thermodynamic model AIOMFAC: calculation of activity coefficients for organic-inorganic mixtures containing carboxyl, hydroxyl, carbonyl, ether, ester, alkenyl, alkyl, and aromatic functional groups. *Atmos. Chem. Phys.* **2011**, *11* (17), 9155–9206.
- (46) Biskos, G.; Paulsen, D.; Russell, L. M.; Buseck, P. R.; Martin, S. T. Prompt deliquescence and efflorescence of aerosol nanoparticles. *Atmos. Chem. Phys.* **2006**, *6*, 4633–4642.
- (47) Romakkaniemi, S.; Haemeri, K.; Vaekevae, M.; Laaksonen, A. Adsorption of water on 8–15 nm NaCl and (NH<sub>4</sub>)<sub>2</sub>SO<sub>4</sub> aerosols measured using an ultrafine tandem differential mobility analyzer. *J. Phys. Chem. A* **2001**, *105* (35), 8183–8188.
- (48) Sander, R. Compilation of Henry's law constants (version 4.0) for water as solvent. *Atmos. Chem. Phys.* **2015**, *15* (8), 4399–4981.
- (49) Hodas, N.; Zuend, A.; Mui, W.; Flagan, R. C.; Seinfeld, J. H. Influence of particle-phase state on the hygroscopic behavior of mixed organic-inorganic aerosols. *Atmos. Chem. Phys.* **2015**, *15* (9), 5027–5045.
- (50) Hodas, N.; Zuend, A.; Schilling, K.; Berkemeier, T.; Shiraiwa, M.; Flagan, R. C.; Seinfeld, J. H. Discontinuities in hygroscopic growth below and above water saturation for laboratory surrogates of oligomers in organic atmospheric aerosols. *Atmos. Chem. Phys.* **2016**, 16 (19), 12767–12792.
- (51) Zuend, A.; Seinfeld, J. H. A practical method for the calculation of liquid-liquid equilibria in multicomponent organic-water-electrolyte systems using physicochemical constraints. *Fluid Phase Equilib.* **2013**, 337, 201–213.
- (52) Hodas, N.; Zuend, A.; Schilling, K.; Berkemeier, T.; Shiraiwa, M.; Flagan, R. C.; Seinfeld, J. H. Discontinuities in hygroscopic growth below and above water saturation for laboratory surrogates of oligomers in organic atmospheric aerosols. *Atmos. Chem. Phys.* **2016**, 16 (19), 12767–12792.
- (53) Fast, J. D.; Berg, L. K.; Alexander, L.; Bell, D.; D'Ambro, E.; Hubbe, J.; Kuang, C.; Liu, J.; Long, C.; Matthews, A.; Mei, F.; Newsom, R.; Pekour, M.; Pinterich, T.; Schmid, B.; Schobesberger, S.; Shilling, J.; Smith, J. N.; Springston, S.; Suski, K.; Thornton, J. A.; Tomlinson, J.; Wang, J.; Xiao, H.; Zelenyuk, A. Overview of the HI-SCALE field campaign: a new perspective on shallow convective clouds. *Bull. Am. Meteorol. Soc.* **2019**, *100*, 821–840.
- (54) Hanson, D. R.; McMurry, P. H.; Jiang, J.; Tanner, D.; Huey, L. G. Ambient pressure proton transfer mass spectrometry: detection of amines and ammonia. *Environ. Sci. Technol.* **2011**, *45* (20), 8881–8888.
- (55) Smith, J. N.; Moore, K. F.; McMurry, P. H.; Eisele, F. L. Atmospheric measurements of sub-20 nm diameter particle chemical composition by thermal desorption chemical ionization mass spectrometry. *Aerosol Sci. Technol.* **2004**, 38 (2), 100–110.
- (56) Berkemeier, T.; Huisman, A. J.; Ammann, M.; Shiraiwa, M.; Koop, T.; Poeschl, U. Kinetic regimes and limiting cases of gas uptake and heterogeneous reactions in atmospheric aerosols and clouds: a general classification scheme. *Atmos. Chem. Phys.* **2013**, 13 (14), 6663–6686
- (57) Zobrist, B.; Soonsin, V.; Luo, B. P.; Krieger, U. K.; Marcolli, C.; Peter, T.; Koop, T. Ultra-slow water diffusion in aqueous sucrose glasses. *Phys. Chem. Chem. Phys.* **2011**, *13* (8), 3514–3526.
- (58) Fuchs, N. A.; Sutugin, A. G., High-dispersed aerosols. In *Topics in Current Aerosol Research*; Hidy, G. M., Brock, J. R., Eds.; Pergamon, 1971; p 1.
- (59) Altaf, M. B.; Zuend, A.; Freedman, M. A. Role of nucleation mechanism on the size dependent morphology of organic aerosol. *Chem. Commun.* **2016**, 52 (59), 9220–9223.
- (60) Shiraiwa, M.; Li, Y.; Tsimpidi, A. P.; Karydis, V. A.; Berkemeier, T.; Pandis, S. N.; Lelieveld, J.; Koop, T.; Poschl, U. Global distribution of particle phase state in atmospheric secondary organic aerosols. *Nat. Commun.* **2017**, *8*, 15002.